EUROGRAPHICS 2026 / B. Masia and J. Thies
(Guest Editors)

COMPUTER GRAPHICS *forum*
Volume 45 (2026), Number 2

Supplemental Material: Skeletal-Driven Animation of Anatomical Humans via Neural Deformation Gradients

G. Nolte[1,3†] F. Kemper[1,3†] U. Schwanecke[2] M. Botsch[1,3]

[1]Computer Graphics Group, TU Dortmund University, Germany
[2]Computer Vision and Mixed Reality Group, RheinMain University of Applied Sciences, Wiesbaden, Germany
[3]Lamarr Institute for Machine Learning and Artificial Intelligence, Dortmund, Germany

1. Prism Gradient Operator

We approximate the deformation gradient as constant within a prism as the matrix that best matches the deformation from the undeformed to the deformed prism in a least squares sense. To take into account all points within the prism, we use the FEM shape functions for prisms [ZTZ05].

Let the six vertices of a prism $\mathbf{P} \in \mathbb{R}^{6\times 3}$ be denoted as $\mathbf{P} = (\mathbf{x}_1, \mathbf{x}_2, \mathbf{x}_3, \mathbf{x}_4, \mathbf{x}_5, \mathbf{x}_6)^\mathsf{T}$, with base triangle $(\mathbf{x}_1, \mathbf{x}_2, \mathbf{x}_3)$ and upper triangle $(\mathbf{x}_4, \mathbf{x}_5, \mathbf{x}_6)$ as shown in Figure 1. Then, the interior of the prism consists of all points that can be written as

$$\mathbf{x}(\alpha, \beta, \xi, \mathbf{P}) = \xi(\alpha\mathbf{x}_1 + \beta\mathbf{x}_2 + \gamma\mathbf{x}_3) + (1-\xi)(\alpha\mathbf{x}_4 + \beta\mathbf{x}_5 + \gamma\mathbf{x}_6) \quad (1)$$

with coefficients $(\alpha, \beta, \xi) \in \mathcal{O}$ and $\gamma = 1 - \alpha - \beta$ satisfying

$$\mathcal{O} = \{(\alpha, \beta, \xi)^\mathsf{T} \in \mathbb{R}^3 \mid 0 \le \alpha, \beta, \xi \le 1, \alpha + \beta \le 1\}. \quad (2)$$

For an undeformed prism $\bar{\mathbf{P}} = (\bar{\mathbf{x}}_1, \ldots, \bar{\mathbf{x}}_6)^\mathsf{T}$ and a deformed prism $\mathbf{P} = (\mathbf{x}_1, \ldots, \mathbf{x}_6)^\mathsf{T}$, we approximate the deformation gradient $\mathbf{F} \in \mathbb{R}^{3\times 3}$ as the linear part of the affine function minimizing

$$\min_{\mathbf{F},\mathbf{t}} \int_{\mathcal{O}} \left\| \mathbf{x}(\alpha, \beta, \xi, \mathbf{P}) - \mathbf{F}\,\mathbf{x}(\alpha, \beta, \xi, \bar{\mathbf{P}}) - \mathbf{t} \right\|^2 \mathrm{d}\alpha\,\mathrm{d}\beta\,\mathrm{d}\xi. \quad (3)$$

The optimal translation $\mathbf{t}$ aligns the centroids of both prisms. To compute $\mathbf{F}$, we can therefore restrict our attention to centered prisms only. Introducing the centering matrix

$$\mathbf{C} = \mathbf{I} - \tfrac{1}{6}\mathbf{1}\mathbf{1}^\mathsf{T}, \qquad \mathbf{1} = (1, \ldots, 1)^\mathsf{T}, \quad (4)$$

we define centered vertex matrices $\bar{\mathbf{P}}_c = \mathbf{C}\bar{\mathbf{P}}$ and $\mathbf{P}_c = \mathbf{C}\mathbf{P}$.

Optimizing Equation 3 for $\mathbf{F}$ yields the closed form

$$\mathbf{F}^\mathsf{T} = \left(\bar{\mathbf{P}}_c^\mathsf{T}\mathbf{W}\bar{\mathbf{P}}_c\right)^{-1} \bar{\mathbf{P}}_c^\mathsf{T}\mathbf{W}\mathbf{P}_c, \quad (5)$$

where $\mathbf{W} \in \mathbb{R}^{6\times 6}$ is a symmetric weight matrix with entries

$$W_{ij} = \begin{cases} 4 & \text{if } i = j, \\ 2 & \text{if } i \text{ and } j \text{ share an edge}, \\ 1 & \text{otherwise.} \end{cases} \quad (6)$$

The gradient operator $\mathbf{G} \in \mathbb{R}^{3\times 6}$ is then given as

$$\mathbf{G} = \left(\bar{\mathbf{P}}_c^\mathsf{T}\mathbf{W}\bar{\mathbf{P}}_c\right)^{-1} \bar{\mathbf{P}}_c^\mathsf{T}\mathbf{W}\mathbf{C}, \quad (7)$$

which, by construction, satisfies

$$\mathbf{F}^\mathsf{T} = \mathbf{G}\mathbf{P}. \quad (8)$$

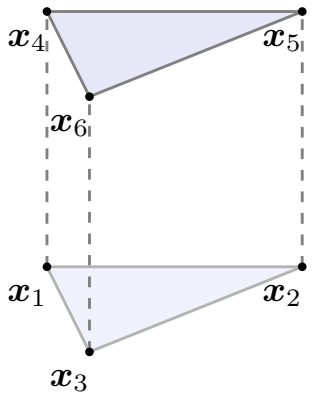

Figure 1: *Configuration of a prism* $\mathbf{P}$.

2. Prism Volume

We compute the signed volume of a prism via the integral over the volume defined by the prism's shape function:

$$\int_{\mathcal{O}} \det(\mathbf{J}(\alpha, \beta, \xi))\,\mathrm{d}\alpha\,\mathrm{d}\beta\,\mathrm{d}\xi \quad (9)$$

$$= \int_0^1 \int_0^1 \int_0^{1-\beta} \det(\mathbf{J}(\alpha, \beta, \xi))\,\mathrm{d}\alpha\,\mathrm{d}\beta\,\mathrm{d}\xi, \quad (10)$$

where $\mathbf{J}$ is the Jacobian of the interpolation function

$$\mathbf{J}(\alpha, \beta, \xi) = \left(\frac{\partial \mathbf{x}}{\partial \alpha}, \frac{\partial \mathbf{x}}{\partial \beta}, \frac{\partial \mathbf{x}}{\partial \xi}\right) \quad (11)$$

and the partial derivatives are given by

$$\frac{\partial \mathbf{x}}{\partial \alpha} = \xi(\mathbf{x}_1 - \mathbf{x}_3) + (1-\xi)(\mathbf{x}_4 - \mathbf{x}_6), \tag{12}$$

$$\frac{\partial \mathbf{x}}{\partial \beta} = \xi(\mathbf{x}_2 - \mathbf{x}_3) + (1-\xi)(\mathbf{x}_5 - \mathbf{x}_6), \tag{13}$$

$$\frac{\partial \mathbf{x}}{\partial \xi} = \alpha(\mathbf{x}_1 - \mathbf{x}_4) + \beta(\mathbf{x}_2 - \mathbf{x}_5) + (1-\alpha-\beta)(\mathbf{x}_3 - \mathbf{x}_6). \tag{14}$$

The determinant of this matrix is quadratic in ξ, which occurs in two columns, and linear in α and β, which occur in only one column. The integral can therefore be evaluated exactly using Gauss-Legendre quadrature with two nodes for the integral over ξ and one node for α and β, whose domain forms a triangle. The integral thus evaluates to

$$V = \tfrac{1}{4}\left(\det(\mathbf{J}(\omega_1)) + \det(\mathbf{J}(\omega_2))\right). \tag{15}$$

with nodes

$$\omega_1 = \left(\frac{1}{3}, \frac{1}{3}, \frac{1-\frac{1}{\sqrt{3}}}{2}\right)^\mathsf{T} \text{ and } \omega_2 = \left(\frac{1}{3}, \frac{1}{3}, \frac{1+\frac{1}{\sqrt{3}}}{2}\right)^\mathsf{T}. \tag{16}$$

3. Comparison of Warping Techniques

We compared the barycentric warp used by NDG with the RBF warp that was proposed by Komaritzan et al. [KWB21]. We found that the barycentric warp offers a better trade-off between computational efficiency and deformation quality. The RBF warp requires approximately 5000 centers to achieve good deformation quality, which requires 600 ms per frame, making it unsuitable for real-time applications. We used farthest point sampling for finding the RBF centers. In contrast, our barycentric warp runs in 6.86 ms on an Intel Core i7-12700K CPU. For an RBF warp in this time budget, the kernel count must be reduced to 600 centers. This reduction degrades the warping quality; as shown in Figure 2, the sparse kernel distribution compromises the layer separation.

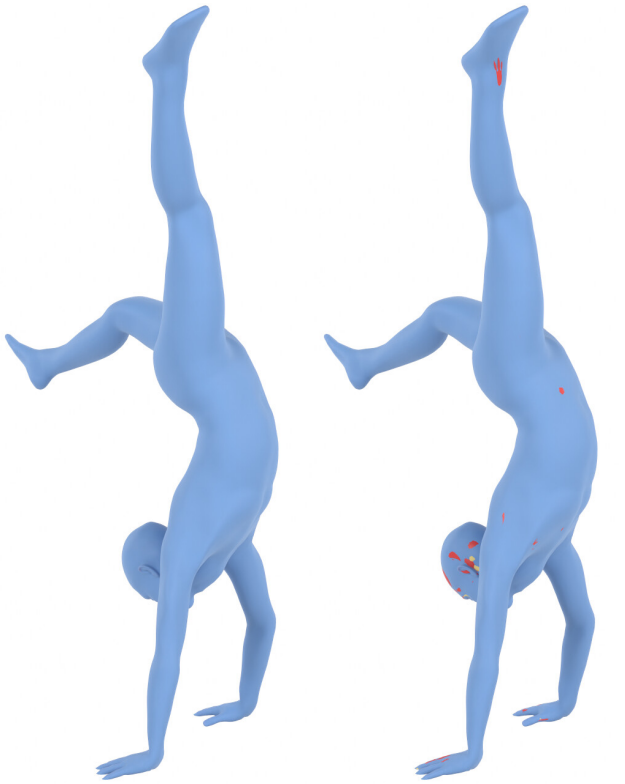

Barycentric warp *RBF warp (600 centers)*

Figure 2: *Comparison of warping techniques. Left: the barycentric warp used by our method maintains the integrity of inner anatomy. Right: RBF warp using 600 kernels. The inner anatomy protrudes through the skin surface.*

References

[KWB21] KOMARITZAN, MARTIN, WENNINGER, STEPHAN, and BOTSCH, MARIO. "Inside Humans: Creating a Simple Layered Anatomical Model from Human Surface Scans". *Frontiers in Virtual Reality* 2 (2021).

[ZTZ05] ZIENKIEWICZ, O.C., TAYLOR, R.L., and ZHU, J.Z. *The Finite Element Method: Its Basis and Fundamentals*. 6th ed. Butterworth-Heinemann, 2005.